Gabrelian, Artem; Miikkulainen, Ville; Ross, Glenn; Paulasto-Kröckel, Mervi

Scaling of piezoelectric in-plane NEMS : Towards nanoscale integration of AlN-based transducer on vertical sidewalls

Published in:
Materials and Design

DOI:
10.1016/j.matdes.2024.113116

Published: 01/08/2024

Document Version
Publisher's PDF, also known as Version of record

Materials & Design 244 (2024) 113116

Contents lists available at ScienceDirect

Materials & Design

journal homepage: www.elsevier.com/locate/matdes

Scaling of piezoelectric in-plane NEMS: Towards nanoscale integration of AlN-based transducer on vertical sidewalls

Artem Gabrelian [a,*], Ville Miikkulainen [b], Glenn Ross [a], Mervi Paulasto-Kröckel [a]

[a] Department of Electrical Engineering and Automation, Aalto University, P.O. Box 13500, FIN-00076 Aalto, Finland
[b] Department of Chemistry and Materials Science, Aalto University, P.O. Box 16100, FI-00076 Aalto, Finland

ARTICLE INFO

Keywords:
Nanoelectromechanical systems
Casimir effect
Aluminum nitride
Switch
Transducer
Scaling

ABSTRACT

One of the key advantages of Piezoelectric MEMS (PiezoMEMS) is its scalability, overcoming issues commonly associated with alternative transduction methods. However, the breadth and depth of studies on scaling the fabrication process from PiezoMEMS to NEMS (Nano-Electro-Mechanical Systems) remain limited. Effective MEMS miniaturization not only improves energy efficiency and surface area reduction but also enables the coupling of nanoscale physics, particularly Casimir Forces, with the NEMS design, device operation, and fabrication opportunities. Here, combined with the finite element method (FEM) modeling, the experimental aluminum nitride (AlN) nanotransducer fabrication is performed to address the fabrication challenges with beam-based in-plane nanostructures and to develop the piezoelectric NEMS design utilizing a controllable stiction behavior. The FEM modeling demonstrates that the designed structure featuring a 220 nm thick silicon (Si) beam with AlN layers located on vertical sidewalls exhibits controllable jump-to-contact and jump-off-contact behaviors. Based on modeling results, a complete piezoelectric sidewall transducer structure is fabricated. The final transducer represents a patterned Si nanobeam with the Molybdenum-AlN-Aluminum transducer located on the vertical sidewalls. The presented findings not only open new opportunities in the piezoelectric MEMS scaling but also establish a platform for the design of innovative "more-than-a-Moore" devices, such as in-plane mechanical latching switches.

1. Introduction

For the past few decades, MEMS devices have been established as powerful platforms for high-precision sensing and actuation in the semiconductor industry [1,2]. Yet, one of the main MEMS development paths is device scaling, leading to a more extensive integration of NEMS technology [3–5]. Scaling from the microscale to the nanometer range is mainly driven by dual objectives: enhancing MEMS performance and exploitation of nanoscale physics phenomena in MEMS design [6,7]. In recent years, various studies have assessed the efficacy of transitioning towards ultra-miniaturized electromechanical devices, with a focus on reducing power consumption, expediting response times, and achieving exceptional sensitivities at high resonant frequencies (MHz-GHz) [7–9]. Amidst these prospects, piezoelectricity has emerged as one of the most promising approaches for sensing and actuation in NEMS [10]. Recent advances in piezoelectric miniaturization constitute a wide variety of applications: nanoelectromechanical relays [11,12], energy harvesters [13], and RF resonators [12].

To date, the prevailing trends in NEMS research and development have been dominated by out-of-plane structures due to the established nanoscale surface micromachining fabrication techniques, such as out-of-the-plane cantilevers [14,15]. In these structures, based on the out-of-the-plane bending, a deposited layer of piezoelectric material on a flat surface plays an integral role in the overall device's output. Consequently, substantial scaling of the surface area becomes unavoidably interrelated with a compromise in the device's overall performance [16,17]. Moreover, this approach naturally limits possibilities for fabricating nanoscale electromechanical circuits. In-plane motion more naturally allows for the integration of nanoelectromechanical circuits, such as switching [18] or precise control of surface-surface interactions [19].

Traditional surface micromachining has been well-established on the MEMS level providing robust processes with CMOS compatibility and batch production capabilities. Even though nanobeam formation in silicon has been comprehensively studied, traditional 'top-down' techniques are not always fully transferable into in-plane nanotransducer

* Corresponding author.
E-mail address: artem.gabrelian@aalto.fi (A. Gabrelian).

https://doi.org/10.1016/j.matdes.2024.113116
Received 3 May 2024; Received in revised form 4 June 2024; Accepted 23 June 2024
Available online 24 June 2024

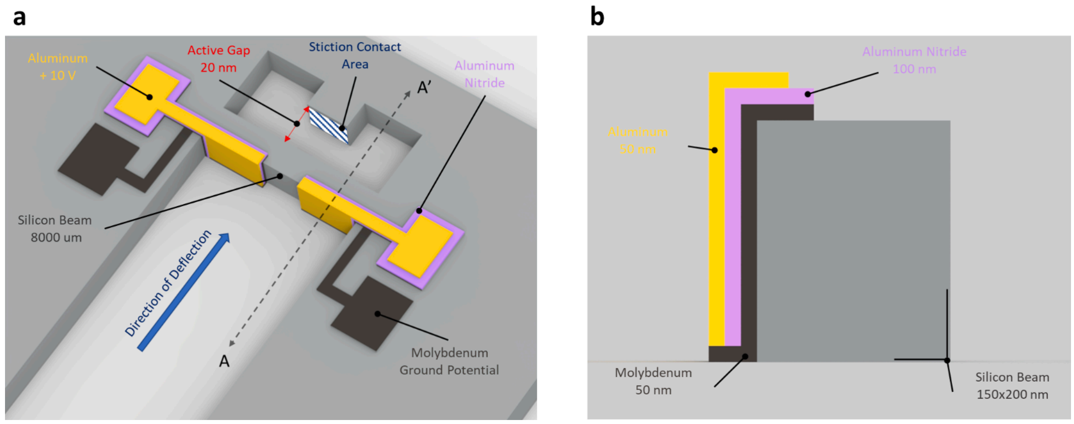

Fig. 1. Overview of the NEMS AlN-based in-plane transducer. a) Isometric view, b) Cross-sectional view.

fabrication. Unlike the conventional piezoelectric MEMS/NEMS fabrication, the in-plane structure necessitates a 'cavities-first' approach, where the first step is the etching of the Si device layer, which is then followed by a substantial materials deposition on the vertical sidewalls. While anisotropic dry etching techniques make it possible to form a nanobeam in a silicon device layer with a reliable process and reproducible structures [9], the need for patterned active piezoelectric material on the sidewalls with integrated top and bottom electrodes imposes certain limitations on deposition techniques or material selection. Within the research on piezoelectric M/NEMS, aluminum nitride (AlN) has proven to be a very promising material for in-plane transducer design due to its availability of various deposition techniques, and CMOS compatibility. Moreover, advanced deposition methods such as metal–organic-chemical-vapor-deposition (MOCVD) [20] and atomic layer deposition (ALD) [21] allow the implementation of AlN layer on vertical sidewalls, which plays a pivotal role in reaching the desired in-plane transducer behavior [22].

However, some uncertainties arise towards the full integration of highly efficient in-plane piezoelectric devices at the nanoscale. The first crucial aspect of the scaling transition lies in the shift of influence from volume-based interactions to surface-based interactions [23]. Even though nanoscale forces such as Van der Waals and, in specific cases, Casimir forces have already been measured experimentally, their practical usage has still not been widely exploited in NEMS design. The proposed transducer concept is aimed to use these forces to imitate a latching relay with a controllable stiction feature. Subsequently, the coupling of in-plane motion, AlN deposition, and utilization of surface interactions places strict NEMS design constraints such as the necessity of parallel motion and the presence of contact area. Thus, the double-clamped beam structure emerges as the most viable approach that combines scaling opportunities with the potential for parallel motion. Nevertheless, the introduction of piezoelectric materials, such as AlN, brings forth additional challenges, such as the crystallographic orientation and the piezoelectric response. The unpatterned AlN layer on the fixed silicon beam proves ineffective in generating meaningful in-plane displacement, as the material lacks the ability to contract along the sidewall. Moreover, in order to exploit the correct contact behavior, the parallel plate or in-plane motion must be maintained while minimizing the out-of-plane component. However, by utilizing ALD deposition, known for its conformal coverage, it is difficult to confine AlN growth to the vertical surfaces leading to parasitic film growth and unwanted deflection response. Another group of challenges lies in the nanofabrication techniques themselves, as conventional MEMS processing methods may not be directly applicable to nanoscale dimensions [24]. For instance, the deposition of high-aspect-ratio layers on vertical sidewalls prohibits the use of more traditional high-resolution patterning techniques, such as lift-off.

In this work, by focusing on the nanofabrication of a piezoelectric multilayer sidewall structure of the AlN-based in-plane transducer, we aim to investigate the scaling mechanism behind in-plane piezoelectric NEMS process integration. To unleash the potential of the proposed structure, comprehensive finite-element modeling (FEM) was performed in the COMSOL multiphysics (COMSOL) software package. Modeling results consider nanoscale interactions such as Casimir Forces and utilize them in the latching switch device realization. Furthermore, the AlN nanotransducer structure was fabricated using EBL lithography and ALD deposition techniques in the dimension ranges based on the modeling results. Finally, the fabricated structure was characterized by focused ion beam/scanning electron microscope (FIB/SEM) techniques with the subsequent transmission electron microscopy (TEM) analysis of the deposited and patterned thin films.

2. Piezoelectric transducer design

In order to comprehensively study the scaling prospects of MEMS piezoelectric devices, the proposed transducer structure based on piezoelectric thin film on vertical sidewalls is introduced. The potential device's configuration is based on a piezoelectric unimorph actuator and consists of a double-clamped silicon beam with the sandwiched AlN layer between the top and bottom metal electrodes. As depicted in Fig. 1 the structure breakdown reveals that AlN vertical thin films are isolated from each other by means of the etched area in the middle of the beam. This separation of piezoelectric thin films is pivotal in facilitating in-plane parallel motion, a critical aspect of the device's operation with a beam structure. The deposition of aluminum and molybdenum for the upper and lower electrodes, respectively allows potential differences across the AlN layers when a voltage is applied. Two distinct design solutions were implemented to investigate the challenges that emerge during the transition of fabrication processes to the nanoscale. The first one involved the utilization of a double-clamped beam structure. While the traditional piezoelectric cantilever design with a single fixed end has been widely established and proven effective, it lacks the capability to facilitate parallel plate motion, which is essential for studying precise nanoscale surface interactions [25]. Therefore, with the unpatterned double-clamped beam structure, the only contribution to the displacement is a strain generated from the non-fixed areas which could be only on the top and bottom of the beam. Ultimately it results in almost the absence of the desired parallel plate motion and necessitates a modification, involving the removal of the central portion of the beam, thereby leaving two AlN areas near the fixed ends. The second feature of the proposed design concept is a flat stiction contact area separated from the transducer beam with a narrow gap (20–200 nm). Notably, this structure allows us to capture and study the complexities of the surface interaction phenomenon. While AlN thin films on one side of the beam drive the structure towards a fixed flat area, it is possible to observe the impact of the stiction or even Casimir Forces on the transducer behavior.

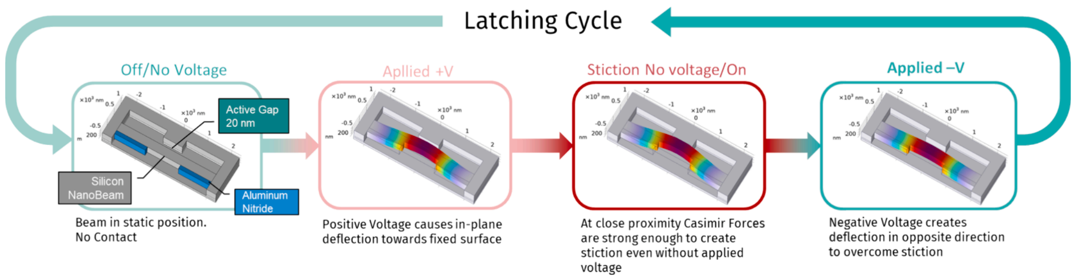

Fig. 2. The operational principle of the proposed NEMS-based latching switch.

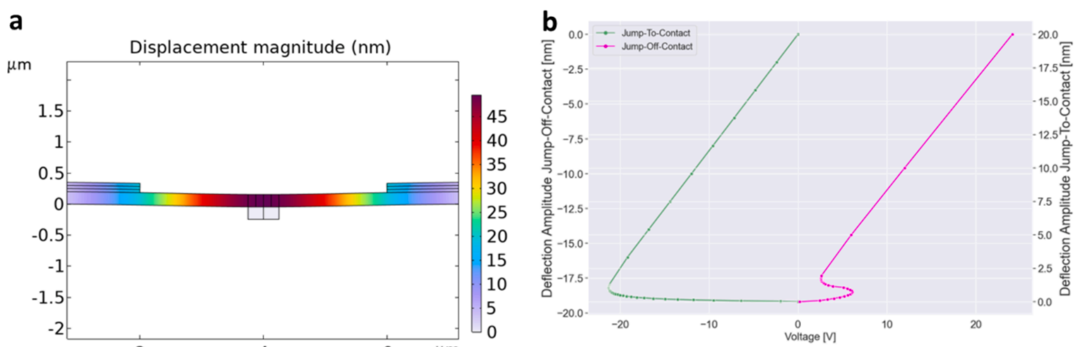

Fig. 3. Modeling of the NEMS in-plane AlN latching switch. a) Displacement Distribution at an equilibrium point. b) Jump-to-contact and jump-off-contact.

Ultimately, the utilization of surface forces can lead to completely novel design approaches in NEMS. For instance, Fig. 2 demonstrates a proposed design of a NEMS switch device. Initially, the switch is considered to be in the "OFF" position: no voltage is applied, and the gap between the fixed and movable area shows the open circuit condition. Then, by increasing the applied voltage on AlN sidewall layers, the beam deflects towards the contact area. At close proximity (<10 nm) jump-to-contact effect occurs: surface interactions are strong enough to overcome the beam's elastic restoration force resulting in stiction contact even without applied voltage on AlN. Eventually, to bring the beam back to the initial state from the "On" position, the opposite voltage signal is applied overcoming the stiction with the piezoelectric actuation and elastic restoration force together.

3. Results and discussion

3.1. Modelling

In order to lay the groundwork for further transducer fabrication and understand the set of scaling challenges, a comprehensive FEM modeling was conducted. The simulations were performed in the COMSOL Multiphysics software package. Fig. 3 depicts the model breakdown with the introduced boundary conditions. As shown, the silicon beam is fixed from both ends with the two separated AlN thin film-based transducers. In turn, to reach the in-plane motion behavior of the transducer it is required to orientate the piezoelectric layers perpendicularly to vertical surfaces. This can be reached by means of setting additional rotated coordinate systems for each dedicated AlN layer, where the z and y axes are flipped on 90 degrees to imitate the correct growth direction of AlN of vertical sidewalls. The AlN wurtzite-type structure's elastic-stiffness coefficients, acquired through experimentation, are represented as a stiffness tensor matrix. With the stress-piezoelectric constants, these anisotropic parameters are utilized to define modelled material as a piezoelectric [26,27]. The model contains a multilayer structure Si-Mo-AlN-Al, where the top surface of Mo serves as ground potential with the voltage applied to the bottom border of Al. Surface interactions in the simulations are introduced by adding a contact boundary condition between moving and fixed areas, while the Casimir Force is applied as a pressure to the contact area. Casimir Force is set up with a distributive behavior through the contact area, having a maximum at the tipping point and a minimum at the starting point of the contact. It has already been reported that starting from the fundamental Casimir Force equation (1) and culminating with the Lipschitz theory of electrodynamic interactions, including material-specific corrections, it is possible to reach relatively accurate estimations of the Casimir force [28–31]. Similarly, as in Equation (1), the stiction force in the model behaves as a gap-dependent pressure, where $\hbar$ is Planck's constant ($h/2\pi$), c is the velocity of light, and d is gap distance.

$$F_{cas} = \frac{\pi^2}{240}\frac{\hbar c}{d^4}\left[\frac{N}{m^2}\right] \tag{1}$$

Simulation results showed that it is possible to couple piezoelectric transduction with the surface physics at the nanoscale with the optimal choices of dimensions. Through the transducer's operation, the structure is balanced between three different forces: surface attraction expressed as Casimir force, elastic restoration of the deformed beam, and the piezoelectric actuation. According to simulated results in Fig. 3a, with the initial 20 nm gap, the jump-to-contact point, where Casimir Forces are strong enough to create stiction, can be observed at 21 V. Moreover, when the gap distance comes closer to 2–4 nm, the Casimir force becomes strong enough to overcome the elastic restoration of the beam. At this point, we can assume that the moving beam's surface will be in contact with the fixed electrode even without applied voltage. In contrast, to validate the capability of the proposed piezoelectric transducer in harnessing the latching feature of NEMS and ensuring controlled jump-to-contact conditions, the opposite FEM study was conducted. Specifically, we reduced the gap to the point of contact and estimated the requisite voltage amplitude necessary to overcome stiction effects. The results, as depicted in Fig. 3b, reveal that a voltage of 5 V is sufficient to break the Casimir stiction. Notably, this simulation represents the worst-case scenario, as it does not account for elastic restoration effects. Ideally, the pre-deformed cantilever will require less voltage because elastic force will have the same direction as the

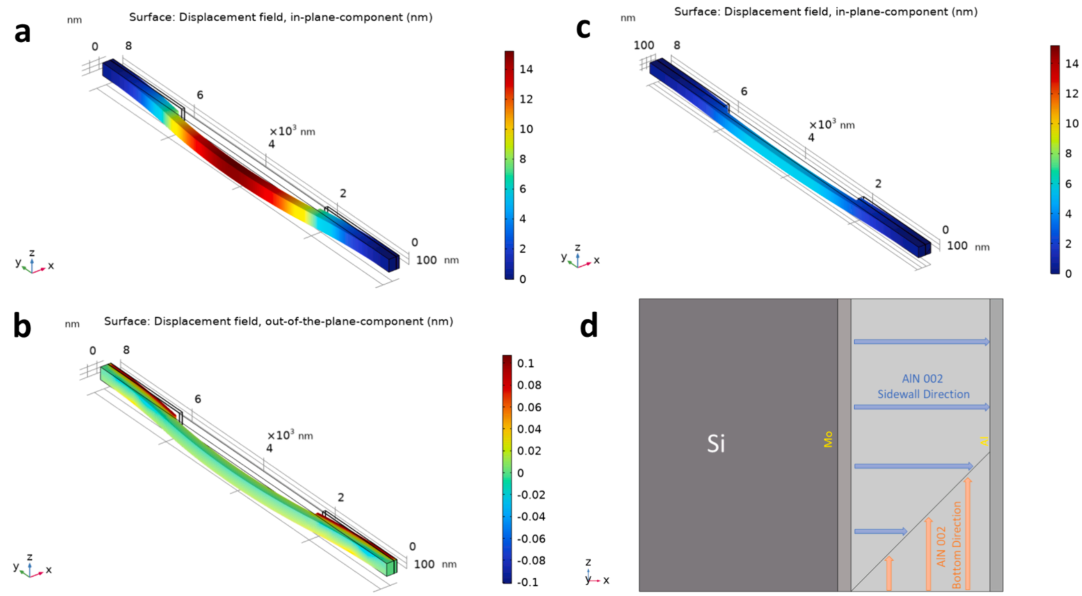

Fig. 4. 3D-Modelling of the piezoelectric nanobeam with the double-clamped structure under applied 10 V (visual deformation amplitude is upscaled). a) In-plane Displacement component. b) Out-of-the-plane displacement component. c) Displacement magnitude of the imitated ALD-deposited thick ALN film with the combined bottom and sidewall growth directions. d) Cross-section of the modelled transducer with the area of combined orientations.

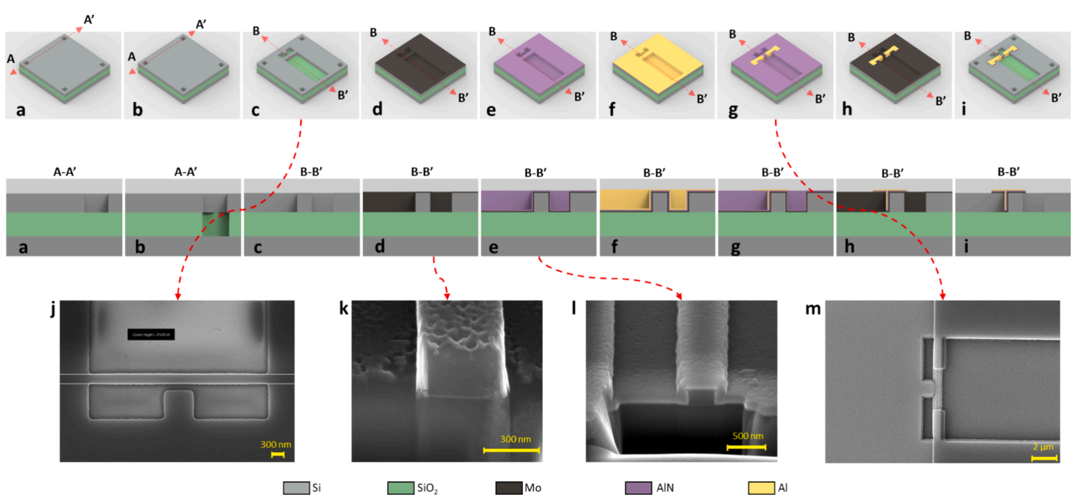

Fig. 5. Nanofabrication process of the in-plane AlN-based nanotransducer. Fabrication flow and SEM images of the key steps.

piezoelectric force.

One of the key guarantees of the correct latching operation cycle is the near-perfect condition of the parallel plate motion. Any significant additional displacement components complicate the jump-to-contact effect caused by surface forces. In the proposed design, the main drivers of the generated beam deflection are the piezoelectric tensors (d_{31}, d_{32}), which are responsible for the stress generated perpendicular to the applied electric field. However, a transducer's structure mainly determines the actuated piezoelectric nanobeam's deflection behavior and its bending direction. The unwanted out-the-plane motion component is limited primarily by a significant difference between the two geometrical aspect ratios: length to thickness (high – facilitates in-plane motion), and width to thickness (low – prevents out-of-the-plane bending). 3D-representation of the double-clamped beam modeling shown in Fig. 4a and 4b depicts the comparison between the in-plane and out-of-plane displacement components validating only a minor presence of the unwanted z-axis deflection with almost no impact on the contact area of the beam.

The model with the increased AlN thickness and combined orientations from ALD has been simulated to bring the design concept closer to the development stage of the fabrication process. Fig. 4c demonstrates that the addition of unwanted growth components together with the thicker AlN thin film results in a considerable reduction of the overall in-plane displacement amplitude. Fig. 4d illustrates the cross-section of the modelled transducer area, where the AlN region is divided into two domains with different crystal orientations: sidewall c-axis orientation (dominant), and c-axis orientation from the bottom area (unwanted). To imitate combined orientations, these two piezoelectric domains have their own designated mutually perpendicular coordinate systems.

Nevertheless, the overall transducer's deflection keeps the desired in-plane direction. Notably, the impact of the additional orientation and unwanted growth should be minimized through the deposition and patterning of the thinner AlN layer.

3.2. Fabrication

The piezoelectric sidewall in-plane nano transducer was fabricated

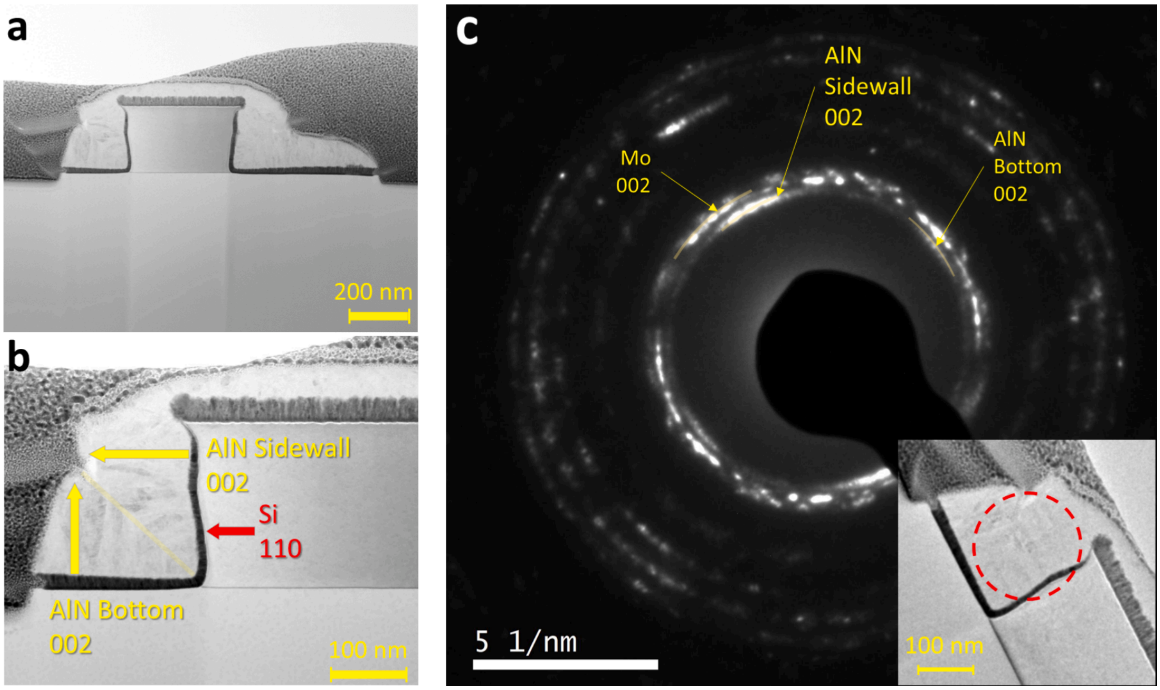

Fig. 6. Cross-sectional STEM images of the fabricated nano AlN-based transducer and obtained SAED of the sidewall structure. a) STEM micrograph of the nano-transducer's cross-section (SiO_2-Si-Mo-AlN-Al). b) Zoomed-in STEM cross-section showing AlN columnar growth on the sidewall. c) SAED pattern of the Si/Mo/AlN/Al structure.

using a CMOS-compatible nanofabrication process, including a combination of electron-beam lithography and dry etching methods, as depicted in Fig. 5. Traditionally the patterning of metal electrodes is mostly concentrated around an out-of-the-plane design approach of Piezoelectric NEMS devices [11,32]. This design allows to leverage the lift-off technique in the patterning of metal and piezoelectric layers. However, this method is not suitable, where high-aspect-ratio sidewall structures play a crucial role. Instead, in the proposed transducer each patterning step requires a complete etching process with the photoresist mask.

Based on modelling results for transducer fabrication Silicon-on-insulator substrate with 220 nm device layer of Silicon and 2 μm of the buried oxide (BOX) layer was selected. Since the sidewall structure involves the pattering of several layers with multiple masks, precise alignment marks formation plays a pivotal role in the nanotransducer process. There are two strategies to utilize alignment in EBL: 1) to have a sufficiently high material (atomic number) contrast, and 2) to exhibit a sufficiently high vertical surface topography (at least 2 μm to be visible at 100 kV electrons). The fabrication started with the second method to fully take advantage of the utilization of SOI structure as depicted in Fig. 5: a) Precise alignment marks cavities in Si device layer were etched in cryogenic mode with SF_6 plasma through AR-P 6200 photoresist mask; b) SiO_2 BOX etching was performed in BHF solution to reach high vertical surface difference; c,j) Nano-beam formation by cryogenic plasma etching of Si device layer; d,k) 50 nm of the Mo was deposited by stage tilting sputtering process to form uniform step coverage of the bottom electrode; e,l) c-axis orientated AlN film was deposited through atomic layer deposition (ALD) with in-situ atomic layer annealing which previously showed significant crystal quality improvement of AlN on vertical sidewalls [20]; f) 50 nm of Al was evaporated with stage tilting process to form top electrode; g,m) etching of Al layer with the AR-P 6200 photoresist mask by combination of BCl_3 and Cl_2 plasma; h) etching of AlN in Ar + Cl_2 plasma chemistry; i) bottom Mo layer was etched by means of CF_4 + O_2 plasma process to form a complete transducer structure.

3.3. Characterization

To systematically study the structure of the fabricated nano-transducer, Transmission electron microscopy (TEM), Scanning transmission electron microscopy (STEM), and selected area electron diffraction (SAED) were used. Fig. 6 depicts both bright field (BF) STEM micrographs as well as SADP. STEM analysis confirmed that the combination of high-resolution EBL and dry etching techniques allows the complete multilayer transducer structure on the vertical sidewalls. AlN thin films on vertical sidewalls as a key structure in the proposed nanoscale transducer design can be characterized mainly by the following figures of merit: conformity and crystal orientation. Firstly, the non-uniform AlN film on the vertical surface may result in parasitic cross-talk between non-lateral motion, compromising the overall efficiency of the device. As shown in Fig. 6b, conformal deposition allows the piezoelectric thin film to coat and, furthermore, pattern complex sidewall surfaces uniformly. When it comes to the AlN crystal quality, the deposited thin film must keep the c-axis orientation perpendicular to the underlying surface for the highest electromechanical coupling. Fig. 6b shows that implemented ALD deposition with in-situ atomic layer annealing allows to reach crystalline AlN with a columnar structure in the growth direction. Previously reported results have shown that in addition to improvements by in-situ plasma annealing in the ALD process, AlN crystal quality also strongly relies on the careful material selection of the underlying layer. Thus, earlier observations revealed that the best crystal quality of AlN was achieved on the Al layer with a (111) orientation [20]. Ultimately, the presented STEM results demonstrate that the integration of molybdenum into the nano-transducer process could be driven not only by the fact that it is a traditional electrode material but also by being a promising candidate for achieving c-axis orientated AlN on vertical sidewalls. The SADP seen in Fig. 6c shows that the AlN grown on the sidewall exhibits strong c-axis preferential orientation perpendicular to the growth surface, necessary for good piezoelectric response. The considerable thickness of AlN in relation to the Si device layer (~120–140 nm vs 220 nm) played a vital role in the presence of both equal components of 002 direction from the

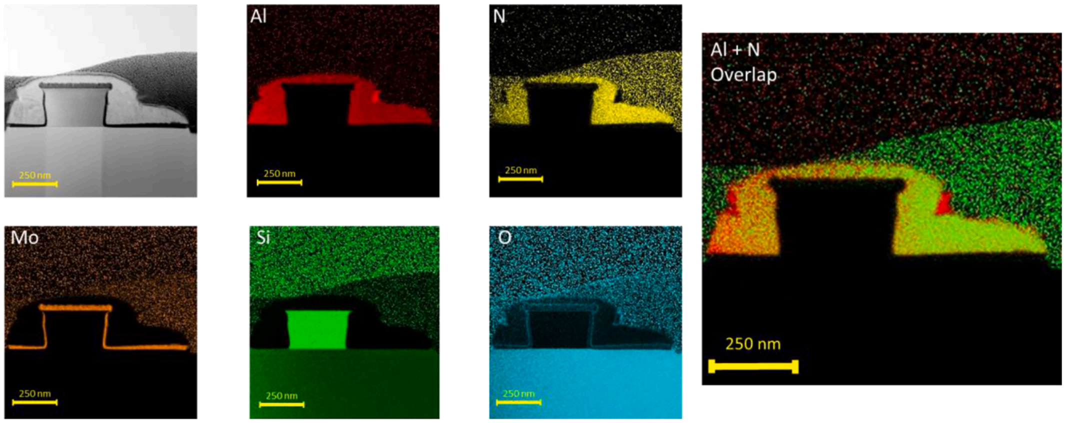

Fig. 7. TEM EDS maps of the SiO2 (BOX)-Si-Mo-AlN-Al material composition of the fabricated nanotransducer.

bottom and sidewall surfaces respectively.

Energy-dispersive X-ray spectroscopy (EDS) analysis was undertaken to perform accurate mapping of the material composition on the sidewalls of the nanotransducer interface. Fig. 7 depicts the color maps of all deposited and patterned materials. Results revealed that the planned Si-electrode-AlN-electrode structure is reached on vertical sidewalls. However, despite the fact that Al top electrode thickness is not uniform around the patterned surface, the key sidewall area, which ultimately will be utilized in the in-plane actuation, is present.

4. Conclusion

In summary, we propose to unlock the scaling potential of MEMS through the innovative design, modeling, and fabrication of a nanoscale in-plane-based transducer structure. To demonstrate the coupling of nanoscale physics and the double-clamped beam structure with vertical piezoelectric sidewalls we introduce the latching mechanism with the controllable jump-to-contact phenomena. The conducted modeling validates that the right balance between the active piezoelectric actuation, elastic restoration, and Casimir forces culminates in the mechanical switch behavior featuring controllable jump-to-contact/jump-off-contact conditions. Based on the modelling results, the nanotransducer was fabricated utilizing a Si/Mo/AlN/Al material stack. The nanofabrication process reveals the successful realization of a multilayer piezoelectric structure on vertical sidewalls on 220 nm device layer SOI chips. The multilayer patterning involved separate steps for each dedicated layer due to the incompatibility of the lift-off technique with the in-plane structure. The deposition of AlN was conducted using the ALD method with the in-situ plasma annealing, while by means of physical vapor deposition the top and bottom electrodes were fabricated, Al and Mo respectively. STEM characterization further underscores the promising quality of the c-axis orientation of the ALD AlN layer with the distinguishable growth directions perpendicular to the sidewall and bottom surfaces and demonstrates the potential of Mo as an underlying layer. This study provides a promising approach towards broadening the scope to full-scale in-plane NEMS integration.

5. Experimental section

FEM Simulation: FEM Simulation was performed in the COMSOL Multiphysics software package with the Solid Mechanics and Electrostatics modules. The beam dimensions: width – 200 nm, thickness – 250 nm, length – 8 μm, AlN layer thickness: 50 nm. Contact area width: 250 nm. The AlN elasticity and coupling matrices were assumed based on experimental data [26,27], the mass density was $\rho = 3300$ kg m^{-3}, and the relative permittivity was $\varepsilon_r = 9$. In-plane AlN orientation was implemented through the built-in base vector system (XZ-plane). The fixed boundary condition was applied to both sides of the beam, while the contact pair was defined between the beam's middle area and the fixed contact surface. The potential difference was applied to the AlN layer to create parallel motion and the Casimir Force was set up as a gap-dependent pressure expressed by equation (1).

NanoTransducer Fabrication: 400 nm of AR-P 6200 EBL resist was spin-coated to a SOI chip with 220 nm of device layer. The alignment marks were patterned by a 100 keV EPBG5000pES EBL system with a 400 μC cm^{-2}. Exposure was followed by a development in the AR 600–546 solution for 1 min and IPA for 30 sec. Si etching was performed by inductively coupled plasma (ICP) cryogenic process with SF_6 and O_2 gases. Then 2 μm of buried oxide layer was removed in the 1:10 HF mixture. For the beam formation, the same lithography + Si etching steps were repeated. Then 50 nm layer of Mo was deposited by magnetron sputtering with a 70 deg tilt, followed by ALD deposition of AlN. ALD was done following the procedure described in previously reported studies [20]. In turn, for the top electrode 50 nm of Al were thermally evaporated. All further patterning steps utilized the same AR-P 6200 photoresist mask with the mentioned before the EBL process. Finally, three subsequent etching processes took place: 1) ICP etching of Al in Cl_2 and BCl_3 chemistry, 2) AlN layer was removed in Cl_2 and Ar ICP process, 3) RIE etching of Mo in $CF_4 + O_2$ plasma.

STEM Characterization: First, the sample was prepared in the dual-beam Focused ion beam SEM system JEOL JIB-4700F aiming at electron-transparent lamella. Preliminary the additional layer of Platinum was deposited upon crucial structure to enhance protection during the Ga-ion milling process. Obtained lamella then was imaged in the high-resolution JEOL JEM-2800 microscope.

CRediT authorship contribution statement

Artem Gabrelian: Writing – original draft, Visualization, Software, Investigation, Conceptualization. **Ville Miikkulainen:** Writing – review & editing, Investigation. **Glenn Ross:** Writing – review & editing, Validation, Supervision, Project administration, Methodology, Conceptualization. **Mervi Paulasto-Kröckel:** Writing – review & editing, Supervision, Resources, Project administration, Funding acquisition, Conceptualization.

Declaration of competing interest

The authors declare that they have no known competing financial interests or personal relationships that could have appeared to influence the work reported in this paper.

Data availability

Data will be made available on request.

Acknowledgments

This article was funded by the Academy of Finland's Academy Research Fellows Programme under Project No. 356673. The authors acknowledge the provision of facilities and technical support of Aalto University at OtaNano Nanomicroscopy Center (Aalto-NMC).

References

[1] A.S. Algamili, M.H.M. Khir, J.O. Dennis, A.Y. Ahmed, S.S. Alabsi, S.S. Ba Hashwan, M.M. Junaid, A Review of Actuation and Sensing Mechanisms in MEMS-Based Sensor Devices, Nanoscale Res Lett 16 (2021) 1–21, https://doi.org/10.1186/s11671-021-03481-7.
[2] Yole Intelligence, Status of the MEMS Industry 2023, https://www.yolegroup.com/product/report/status-of-the-mems-industry-2023/ (accessed April 22, 2024).
[3] J. Zhu, X. Liu, Q. Shi, T. He, Z. Sun, X. Guo, W. Liu, O. Bin Sulaiman, B. Dong, C. Lee, Development Trends and Perspectives of Future Sensors and MEMS/NEMS, Micromachines 11 (2019) 7, https://doi.org/10.3390/MI11010007.
[4] T. Cao, T. Hu, Y. Zhao, Research Status and Development Trend of MEMS Switches: A Review, Micromachines 11 (2020) 694, https://doi.org/10.3390/MI11070694.
[5] L. Wei, X. Kuai, Y. Bao, J. Wei, L. Yang, P. Song, M. Zhang, F. Yang, X. Wang, The Recent Progress of MEMS/NEMS Resonators, Micromachines 12 (2021) 724, https://doi.org/10.3390/MI12060724.
[6] R. Yang, J. Qian, P.-X.-L. Feng, R. Yang, J. Qian, P.-X.-L. Feng, Electrodynamic Force, Casimir Effect, and Stiction Mitigation in Silicon Carbide Nanoelectromechanical Switches, Small 16 (2020) 2005594, https://doi.org/10.1002/SMLL.202005594.
[7] T. Tharpe, E. Hershkovitz, F. Hakim, H. Kim, R. Tabrizian, Nanoelectromechanical resonators for gigahertz frequency control based on hafnia–zirconia–alumina superlattices, Nat Electron 6 (2023) 599–609, https://doi.org/10.1038/S41928-023-00999-9.
[8] M. Li, H. Tang, M. Roukes, Ultra-sensitive NEMS-based cantilevers for sensing, scanned probe and very high-frequency applications, Nature Nanotech 2 (2007) 114–120, https://doi.org/10.1038/nnano.2006.208.
[9] Y. Wang, T. Li, H. Yang, Nanofabrication, effects and sensors based on micro-electro-mechanical systems technology, Philosophical Transactions of the Royal Society A: Mathematical, Physical and Engineering Sciences 371 (2013), https://doi.org/10.1098/RSTA.2012.0315.
[10] X. Le, Q. Shi, P. Vachon, E.J. Ng, C. Lee, Piezoelectric MEMS—evolution from sensing technology to diversified applications in the 5G/Internet of Things (IoT) era, Journal of Micromechanics and Microengineering 32 (2021) 014005, https://doi.org/10.1088/1361-6439/AC3AB9.
[11] U. Zaghloul, G. Piazza, Highly scalable NEMS relays with stress-tuned switching voltage using piezoelectric buckling actuators, IEEE Trans Electron Devices 61 (2014) 3520–3528, https://doi.org/10.1109/TED.2014.2331914.
[12] R.B. Karabalin, M.H. Matheny, X.L. Feng, E. Defa, G. Le Rhun, C. Marcoux, S. Hentz, P. Andreucci, M.L. Roukes, Piezoelectric nanoelectromechanical resonators based on aluminum nitride thin films, Appl Phys Lett 95 (2009) 103111, https://doi.org/10.1063/1.3216586/337442.
[13] G. Zhu, R. Yang, S. Wang, Z.L. Wang, Flexible high-output nanogenerator based on lateral ZnO nanowire array, Nano Lett 10 (2010) 3151–3155, https://doi.org/10.1021/nl101973h.
[14] Z. Qian, F. Liu, Y. Hui, S. Kar, M. Rinaldi, Graphene as a Massless Electrode for Ultrahigh-Frequency Piezoelectric Nanoelectromechanical Systems, Nano Lett 15 (2015) 4599–4604, https://doi.org/10.1021/acs.nanolett.5b01208.
[15] D. Dezest, O. Thomas, F. Mathieu, L. Mazenq, C. Soyer, J. Costecalde, D. Remiens, J.F. Deü, L. Nicu, Wafer-scale fabrication of self-actuated piezoelectric nanoelectromechanical resonators based on lead zirconate titanate (PZT), Journal of Micromechanics and Microengineering 25 (2015) 035002, https://doi.org/10.1088/0960-1317/25/3/035002.
[16] N. Sinha, G.E. Wabiszewski, R. Mahameed, V.V. Felmetsger, S.M. Tanner, R. W. Carpick, G. Piazza, Piezoelectric aluminum nitride nanoelectromechanical actuators, Appl Phys Lett 95 (2009) 53106, https://doi.org/10.1063/1.3194148/338267.
[17] M. Rinaldi, C. Zuniga, G. Piazza, 5-10 GHZ ALN contour-mode nanoelectromechanical resonators, Proceedings of the IEEE International Conference on Micro Electro Mechanical Systems (MEMS) (2009) 916–919. Doi: 10.1109/MEMSYS.2009.4805533.
[18] W. Jiang, F.M. Mayor, R.N. Patel, T.P. McKenna, C.J. Sarabalis, A.H. Safavi-Naeini, Nanobenders as efficient piezoelectric actuators for widely tunable nanophotonics at CMOS-level voltages, Communications Physics 2020 3:1 3 (2020) 1–9. Doi: 10.1038/s42005-020-00412-3.
[19] L. Tang, M. Wang, C.Y. Ng, M. Nikolic, C.T. Chan, A.W. Rodriguez, H.B. Chan, Measurement of non-monotonic Casimir forces between silicon nanostructures, Nature Photonics 2016 11:2 11 (2017) 97–101. Doi: 10.1038/nphoton.2016.254.
[20] E. Österlund, S. Suihkonen, G. Ross, A. Torkkeli, H. Kuisma, M. Paulasto-Kröckel, Metalorganic chemical vapor deposition of aluminum nitride on vertical surfaces, J Cryst Growth 531 (2020) 125345, https://doi.org/10.1016/J.JCRYSGRO.2019.125345.
[21] E. Österlund, H. Seppänen, K. Bespalova, V. Miikkulainen, M. Paulasto-Kröckel, Atomic layer deposition of AlN using atomic layer annealing—Towards high-quality AlN on vertical sidewalls, Journal of Vacuum Science & Technology A: Vacuum, Surfaces, and Films 39 (2021) 32403, https://doi.org/10.1116/6.0000724/1079708.
[22] K. Bespalova, T. Nieminen, A. Gabrelian, G. Ross, M. Paulasto-Kröckel, In-Plane AlN-based Actuator: Toward a New Generation of Piezoelectric MEMS, Adv Electron Mater 9 (2023), https://doi.org/10.1002/AELM.202300015.
[23] S. (Salvatore) Baglio, Salvatore. Castorina, N. Savalli, Scaling issues and design of MEMS, John Wiley & Sons, 2007.
[24] P. van Assenbergh, E. Meinders, J. Geraedts, D.P. Dodou van Assenbergh, D. Dodou, E. Meinders, J. Geraedts, Nanostructure and Microstructure Fabrication: From Desired Properties to Suitable Processes, Small 14 (2018) 1703401, https://doi.org/10.1002/SMLL.201703401.
[25] M. Wang, L. Tang, C.Y. Ng, R. Messina, B. Guizal, J.A. Crosse, M. Antezza, C. T. Chan, H.B. Chan, Strong geometry dependence of the Casimir force between interpenetrated rectangular gratings, Nature Communications 2021 (12) (2021) 1–9, https://doi.org/10.1038/s41467-021-20891-4.
[26] Y. Goldberg, M. Levinshtein, S. Rumyantsev, Properties of Advanced Semiconductor Materials: GaN, AIN, InN, BN, SiC, SiGe, John Wiley & Sons, New York, 2001.
[27] A.F. Wright, Elastic properties of zinc-blende and wurtzite AlN, GaN, and InN, J Appl Phys 82 (1997) 2833–2839, https://doi.org/10.1063/1.366114.
[28] B.V. Derjaguin, I.I. Abrikossova, Direct measurements of molecular attraction of solids, Journal of Physics and Chemistry of Solids 5 (1958) 1–10, https://doi.org/10.1016/0022-3697(58)90126-4.
[29] S.G. Johnson, Numerical methods for computing casimir interactions, Lecture Notes in Physics 834 (2011) 175–218, https://doi.org/10.1007/978-3-642-20288-9_6.
[30] I.E. Dzyaloshinskii, E.M. Lifshitz, L.P. Pitaevskii, The general theory of van der Waals forces, Adv Phys 10 (1961) 165–209, https://doi.org/10.1080/00018736100101281.
[31] H.B. Casimir, On the Attraction between Two Perfectly Conducting Plates, Proc. Kon. Ned. Akad. Wet. 51 (1948) 793-, https://doi.org/10.18914/TRIBOLOGIST.58.02_65.
[32] B.D. Davidson, D. Seghete, S.M. George, V.M. Bright, ALD tungsten NEMS switches and tunneling devices, Sens Actuators A Phys 166 (2011) 269–276, https://doi.org/10.1016/J.SNA.2009.07.022.